

## THE EVOLUTION OF A SEVERE HAILSTORM IN CENTRAL SOUTH CAROLINA

*Michael D. Vescio*  
*National Weather Service Forecast Office*  
*Columbia, South Carolina*

### 1. INTRODUCTION

On 13 March 1991, a severe hailstorm occurred in central South Carolina. The storm originated as a cluster of relatively weak multicell thunderstorms in the western part of the state around 2200 UTC, and evolved into a supercell (based on radar signatures) just south of Columbia (CAE) by 0000 UTC on March 14. The storm produced a hail swath approximately 70 mi long (Figure 1) as it moved east-southeast. Hail, up to 2 1/2 inches in diameter, was reported with the storm in southern Lexington county. Also, golf ball size hail, 4 inches deep, was reported in northern Calhoun county.

This paper will focus on the synoptic and mesoscale features which created an environment favorable for severe weather over South Carolina. An overview of the evolution of the radar echo structure viewed from the WSR-57 radar at Charleston, SC (CHS) will also be presented. Although radar indicated a low-level reflectivity pendant, or hook, for much of its lifetime, there were no reports of tornadoes. However, the storm's path was primarily through sparsely populated areas after dark. Therefore, it is possible that a tornado was spawned, but not observed. The SkewT-Hodograph Analysis

and Research Program (SHARP) (Hart and Korotky 1991) was used to generate hodographs for CHS and Waycross, GA (AYS). Athens, GA (AHN) was not included since it was located in an airmass substantially different from that associated with the severe storm. Storm relative (s-r) helicity was calculated to assess the potential for tornadic development.

### 2. RADAR CHARACTERISTICS

Browning (1964) coined the term "supercell" for a type of storm that produces most, if not all, violent tornadoes, and accounts for a high percentage of hail events. Well known supercell radar echo characteristics include: 1) a sloping overhang echo on the right flank; and 2) a vault that penetrates the overhang echo, often referred to as a Bounded Weak Echo Region (BWER; Chisholm 1973), with a hook that partly surrounds the vault in low levels.

Figure 2 depicts the low-level radar reflectivity (0.5° elevation) viewed from CHS as the storm evolved and moved across the state. At 2230 UTC, a relatively weak multicell cluster was located about 25 mi to the southwest of

CAE. Maximum tops were 26,000 ft, and maximum reflectivity was Video Integrator and Processor (VIP) level 3. The storm cluster was moving from 250° at 35 kt, which approximates the 0-6 km mean wind reported at CHS and AYS. By 0005 UTC on March 14, the convective cluster formed into a single cell just south of CAE. The maximum echo top increased to 42,000 ft, while a strong low level reflectivity gradient was observed along the forward flank of the cell, with the VIP level 5 core displaced along the leading edge. By 0030 UTC (not shown), the storm developed a hook echo, and began moving to the right of the mean wind (from 290° at 35 kt), both characteristics of supercell storms (Klemp 1987). The supercell persisted until around 0130 UTC, when the hook dissipated and the storm began to weaken.

In recent years, Moller and Doswell (1988) and Moller et al. (1990) developed the concept of the High Precipitation (HP) supercell, in which considerable precipitation (heavy rainfall and hail) is observed on the trailing edge, and perhaps leading side of a mesocyclone. Classic supercells often develop radar hook echoes comprised of relatively low reflectivities, whereas HP storms contain broad, high reflectivity hooks. The broad, highly reflective hook is indicative of a mesocyclone wrapped in significant rainfall and hail for an extended period of time. Although they can occur in the Great Plains, the HP supercell predominates in the southern and eastern U.S. In this case, it appears that the severe thunderstorm was an HP supercell since the maximum reflectivity in the radar hook was VIP level 5. Also, the evolution of the storm is similar to a composite life cycle identified with HP supercells developed by Moller et al. (1990). One of the two life cycles presented by Moller et al. (1990) is presented in Figure 3. The radar-

observed life cycle for this case is depicted in Figure 4. The evolution of the supercell appears to be quite similar to the Moller et al. HP supercell evolution (1-7b) shown in Figure 3. Although tornadoes spawned from HP supercells are typically weaker than their classic counterpart, these types of storms frequently deposit destructive hail over a wide area.

As mentioned previously, no tornado was reported. However, during most of the period that a hook echo was observed, the storm was over the nearly uninhabited swamp land along the Congaree River southeast of CAE. In addition, as noted by Moller et al. (1990), spotters often have difficulty discerning tornadoes within HP storms, as they are usually enshrouded in heavy precipitation. This problem could have been enhanced by the fact that the storm occurred after sunset.

### 3. SYNOPTIC FEATURES

Figure 5 is the surface analysis for 0000 UTC, March 14. Low pressure was over eastern Kentucky, with a cold front extending south into northwest Georgia. A slow moving warm front extended across central South Carolina. The highly deformed character of this front to the lee of the Appalachians is indicative of cold-air damming (Forbes et al. 1987; Vescio 1991). A mesoscale low pressure center formed along the Georgia/South Carolina border. The evolution of this low was depicted quite well by the AFOS Data Analysis Program (ADAP; Bothwell 1988), and will be discussed further in the next section.

Figure 6 is the 500 mb height and absolute vorticity for 0000 UTC on March 14. Weak PVA was occurring over South Carolina. Figure 7 is an isotach analysis at 500 mb also valid at 0000 UTC on

March 14. Figure 7 indicates a cyclonically curved jet streak extending from Oklahoma to southern South Carolina. (The jet at 300 mb (not shown) was located a little further west, and was not as well defined.) The severe weather area occurred in the left exit region of the 500 mb jet, which is a location of enhanced divergence. The jet streak was easily visible on the Satellite Weather Information System (SWIS) water vapor imagery as a dark (or dry) streak (not shown). Thus, animation of the water vapor imagery was used to track the progression of the jet maxima.

Figure 8 is an analysis of the dew point depression at 700 mb. A tongue of high dewpoint depressions ( $> 25^{\circ}\text{C}$ ) was evident over the eastern half of South Carolina (dry air at 500 mb was also apparent in Figure 7). Doswell (1982) indicated that dry air at mid-levels may be an important factor for severe thunderstorm development. It may also play a key role in tornadogenesis (Lemon and Doswell 1979).

In summary, several synoptic features favored the development of strong convection. The surface boundary and low pressure provided low-level forcing, whereas PVA and a jet streak at 500 mb enhanced upward vertical motion. Also, the presence of a mid-level dry intrusion increased the potential for severe convection.

## 4. SOUNDING PARAMETERS

### 4.1 Atmospheric Stability

Between 1200 UTC March 13, and 0000 UTC March 14, differential thermal advection destabilized the atmosphere in the threat area. During this time, the temperature at 850 mb increased by  $2^{\circ}\text{C}$  at both CHS and AYS, whereas the 500 mb temperature at each station decreased by  $2^{\circ}\text{C}$  and  $1^{\circ}\text{C}$  respectively. This

advection pattern was apparent in the 1200 UTC upper-air analyses (not shown). Surface heating along and south of the warm frontal boundary also contributed to the destabilization process, allowing convective temperatures (about  $19^{\circ}\text{C}$ ) to be reached.

The magnitude of destabilization was revealed by some of the sounding parameters generated by SHARP for the two locations. At 1200 UTC CHS, had a Lifted Index (LI) of +8, and a Total Totals index (TT) of 37, both indicating stable conditions. However, by 0000 UTC substantial destabilization had occurred as the LI decreased to -3, and the TT increased to 47. For AYS, the 1200 UTC values of LI and TT were -1 and 51, respectively. By 0000 UTC, the LI decreased to -7, and the TT increased to 53. Both these values indicate a high probability of strong convection (NWSTC 1990).

### 4.2 Hodographs

Figure 9 is a hodograph comprised of storm relative wind vectors from the AYS sounding at 0000 UTC on the March 14. The observed storm motion was from  $290^{\circ}$  at 35 kt. A clockwise turning hodograph is indicated, which favors right-moving supercells (Klemp 1987). Based on the observed storm motion, a 0-3 km helicity of  $252 \text{ m}^2\text{s}^{-2}$  was calculated. This is close to the median value of  $278 \text{ m}^2\text{s}^{-2}$  associated with 8 weak tornado (F0-F1) producing storms studied by Davies-Jones et al. (1990). Figure 10 is a 0000 UTC hodograph for CHS. Figure 10 is also characterized by clockwise shear. The s-r helicity was somewhat lower at  $197 \text{ m}^2\text{s}^{-2}$ , but was still within the range of  $150\text{-}299 \text{ m}^2\text{s}^{-2}$  suggested for weak tornadoes by Davies-Jones et al. (1990). Based on this discussion, it appears that the s-r helicity was sufficient in the storm environment to produce a rotating updraft. The presence of a hook echo on radar infers that rotation was occurring in the storm.

## 5. ADAP OUTPUT

Figures 11a-c depict the evolution and progression of the warm-frontal mesolow (Figure 5) by using 2-hourly surface streamline analyses (AFOS graphic SSW) from 2200 UTC on March 13 to 0200 UTC on March 14. The low developed over northeast Georgia and gradually moved into western South Carolina. Although the low center was still in eastern Georgia by 0000 UTC, a broad region of confluence is evident extending east into central South Carolina, where convection initiated. This confluence zone is probably a reflection of the warm (or quasi-stationary) front extending east of this mesolow. The low persisted for several hours after 0200 UTC (not shown) as it moved across northern South Carolina into southeast North Carolina. In fact, additional thunderstorms, some severe, developed near the low after 0100 UTC in northern portions of South Carolina. Golf ball size hail was reported covering the ground in Ridgeway, about 40 miles north of CAE.

Figure 12 is the surface potential temperature (theta) advection (AFOS graphic STA) analysis for 2100 UTC. Strong warm advection was evident over central Georgia extending into central South Carolina. Low-level warm air advection destabilizes the atmosphere, and is associated with synoptic scale upward motion. Another major consequence of low-level warm advection is a veering wind profile in the Ekman layer which enhances the possibility of storm rotation (Davies-Jones 1983).

Note, the theta advection axis and gradient over central and western South Carolina is roughly aligned with the confluence zone in Figure 11a (unfortunately, a 2200 UTC theta advection chart was not available). The presence of a boundary, such as this warm front, can act as an important source of horizontal vorticity (Maddox et al. 1980).

In addition, Moller et al. (1990) noted that HP storms tend to travel along pre-existing or quasi-stationary boundaries. It appears that the HP supercell in this case tracked along the quasi-stationary boundary across South Carolina.

Figure 13 is an analysis of surface moisture flux convergence (AFOS graphic SMC) at 2200 UTC. Moisture flux convergence (MFC) assists with the assessment of thunderstorm potential since this field includes the effects of both mass convergence, which leads to upward vertical motion, and moisture advection, which destabilizes the atmosphere (Waldstreicher 1989). At this time, an MFC maximum was in northeast Georgia with smaller, but still positive, MFC values throughout the threat area. The maximum remained nearly stationary until it shifted into western South Carolina at 0100 UTC on March 14 (not shown).

Based on these ADAP analyses, it might appear that the most favorable area for convection was in central and eastern Georgia, where the strongest warm advection, the highest MFC values, and a mesolow were located. Yet no convection developed in this region. Figure 14 is an ADAP cap strength analysis at 2200 UTC. The capping inversion is very important since it may act as a lid to convection, even if the air below the cap is unstable. Evidence suggests that a critical isopleth of cap strength is  $2^{\circ}\text{C}$  (Graziano and Carlson 1987). Larger values could inhibit or prevent convection. Figure 14 shows that the cap strength was  $3^{\circ}\text{C}$  in the region of highest theta advection and MFC. Bothwell (1988) states that areas of moisture convergence are often capped by an inversion preventing deep convection near the MFC maximum. Carlson et al. (1983) described the process of "underrunning" where the moist air flows to a weak point in the inversion, where storms can develop more easily despite lower values of MFC. Underrunning was apparently important

for this case since the storm developed downwind (relative to the low level flow) of the MFC maximum in an area where the cap was weak. (A 3°C cap persisted through 0000 UTC (not shown) on March 14 over northeast Georgia.)

## 6. SUMMARY

On 13 March 1991 a severe hailstorm struck central South Carolina. The storm originated as a small multicell cluster and evolved into a heavy-precipitation (HP) supercell. Hailstones up to 2 1/2 inches in diameter were reported. The hail depth on the ground was up to 4 inches in some areas. Many features on both the synoptic and mesoscale combined to produce a favorable environment for severe convection.

Although a tornado was not reported with the storm, a low-level hook echo was present for much of its lifetime. Results indicate that the 0-3 km s-r helicity was strong enough, based on the values suggested by Davies-Jones et al. (1990) to result in a weak tornado. It is possible that a tornado occurred, but was not observed since the supercell traversed sparsely populated areas, and was associated with substantial rainfall and hail in the vicinity of the apparent mesocyclone.

This case demonstrates the utility of ADAP for short-term forecasting of severe weather. The ADAP analyses revealed several precursors to severe convection including strong MFC and warm advection. The cap strength analysis identified the area most likely to experience severe weather. The cap was strong enough to prevent deep convection over most of the area that was influenced by warm advection and MFC. The streamline and wind plot captured the evolution of a mesolow moving along the surface warm front.

SWIS also provided some valuable information for this case. The progression of a strong jet streak was monitored on the water vapor imagery loop.

Finally, SHARP is a valuable resource for determining severe weather potential. It has capabilities beyond the AFOS program CONVECT (Stone 1988). For example, soundings and hodographs can be modified quickly as conditions change. The software also computes many indices including low-level s-r helicity and shear that have been determined to be critical for the development of mesocyclones and tornadoes.

## 7. ACKNOWLEDGEMENTS

Many thanks to Ron Przybylinski (SOO, WSFO St. Louis), and Warren Snyder (WSFO Albany) for their insightful comments that substantially improved this manuscript.

## REFERENCES

- Bothwell, P. D., 1988: Forecasting convection with the AFOS Data Analysis Program (ADAP - Version 2.0). NOAA Technical Memorandum NWS SR-122, NOAA/NWS, Fort Worth, TX, 91 pp.
- Browning, K. A., 1964: Airflow and precipitation trajectories within severe local storms which travel to the right of the winds. J. Atmos. Sci., 21, 634-639.
- Carlson, T. N., S. G. Benjamin, G. S. Forbes, and Y. F. Li, 1983: Elevated mixed layers in the regional severe storm environment: Conceptual models and case studies. Mon. Wea. Rev., 111, 1453-1473.
- Chisholm, A. J., 1973: Alberta hailstorms, Part I: Radar case studies and airflow models. Meteorological Monograph No. 14, Amer. Meteor. Soc., Boston, MA, 36 pp.

- Davies-Jones, R., 1983: The onset of rotation in thunderstorms. Preprints, 13th Conf. on Severe Local Storms, Tulsa, OK, Amer. Meteor. Soc., 215-218.
- Davies-Jones, R., D. W. Burgess, and M.P. Foster, 1990: Test of helicity as a tornado forecast parameter. Preprints, 16th Conf. on Severe Local Storms, Kananaskis Provincial Park, Alberta, Canada, Amer. Meteor. Soc., 588-592.
- Doswell, C. A., 1982: The operational meteorology of convective weather - Volume I: Operational mesoanalysis. NOAA Technical Memorandum NWS NSSFC-5, NOAA/NWS/NSSFC, Kansas City, MO, 135 pp.
- Forbes, G. S., R. A. Anthes, and D. W. Thompson, 1987: Synoptic and mesoscale aspects of an Appalachian ice storm associated with cold-air damming. Mon. Wea. Rev., 115, 564-591.
- Graziano, T. M., and T. M. Carlson, 1987: A statistical evaluation of lid strength on deep convection. Wea. Forecasting, 2, 127-139.
- Hart, J. A. and J. Korotky, 1991: The SHARP workstation v1.50 User's Manual. NOAA/NWS, Charleston, WV 30 pp.
- Klemp, J. B., 1987: Dynamics of tornadic thunderstorms. Ann. Rev. Fluid Mech., 33 pp.
- Lemon, L. R., and C. A. Doswell, 1979: Severe thunderstorm evolution and mesocyclone structure as related to tornadogenesis. Mon. Wea. Rev., 107, 1184-1197.
- Maddox, R. A., L. R. Hoxit, and C. F. Chappel, 1980: A study of tornadic thunderstorm interactions with thermal boundaries. Mon. Wea. Rev., 108, 322-336.
- Moller, A. R. and C. A. Doswell, 1988: A proposed advanced storm spotters' training program. Preprints, 15th Conf. on Severe Local Storms, Baltimore, MD, Amer. Meteor. Soc., 173-177.
- Moller, A. R., C. A. Doswell, and R. Przybylinski, 1990: High-precipitation supercells: A conceptual model and documentation. Preprints, 16th Conf. on Severe Local Storms, Kananaskis Park, Alberta, Amer. Meteor. Soc., 52-57.
- National Weather Service Training Center, 1990: Severe Convective Storms. NWS/NOAA, Kansas City, MO, 173 pp.
- Stone, H. M., 1988: Convective parameters and hodograph program - COVECTA and CONVECTB. NOAA Eastern Region Computer Programs and Problems NWS ERCP 37 Revised, National Weather Service, Bohemia, NY, 44 pp.
- Vescio, M. D., 1991: A heavy rainfall and severe weather episode in Central South Carolina. Part 1: Synoptic features leading to heavy rainfall. Eastern Region Technical Attachment 91-4B, NOAA/NWS, Bohemia, NY, 8 pp.
- Waldstreicher, J. S., 1989: A guide to utilizing moisture flux convergence as a predictor of convection. Nat. Wea. Digest, 14, 20-35.

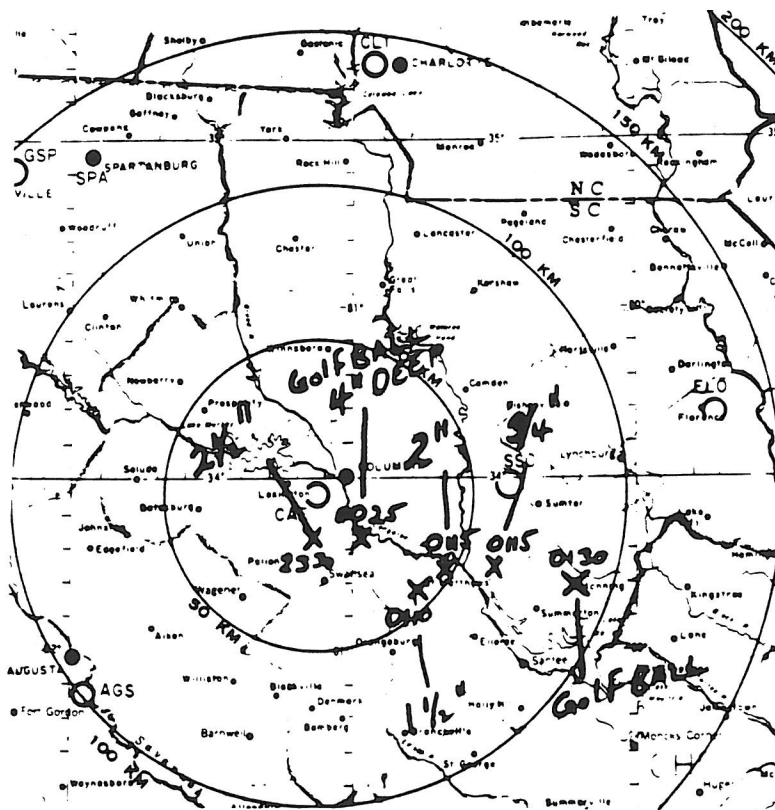


Figure 1. Time (UTC), location (x), and size (inches) of large hail reports.

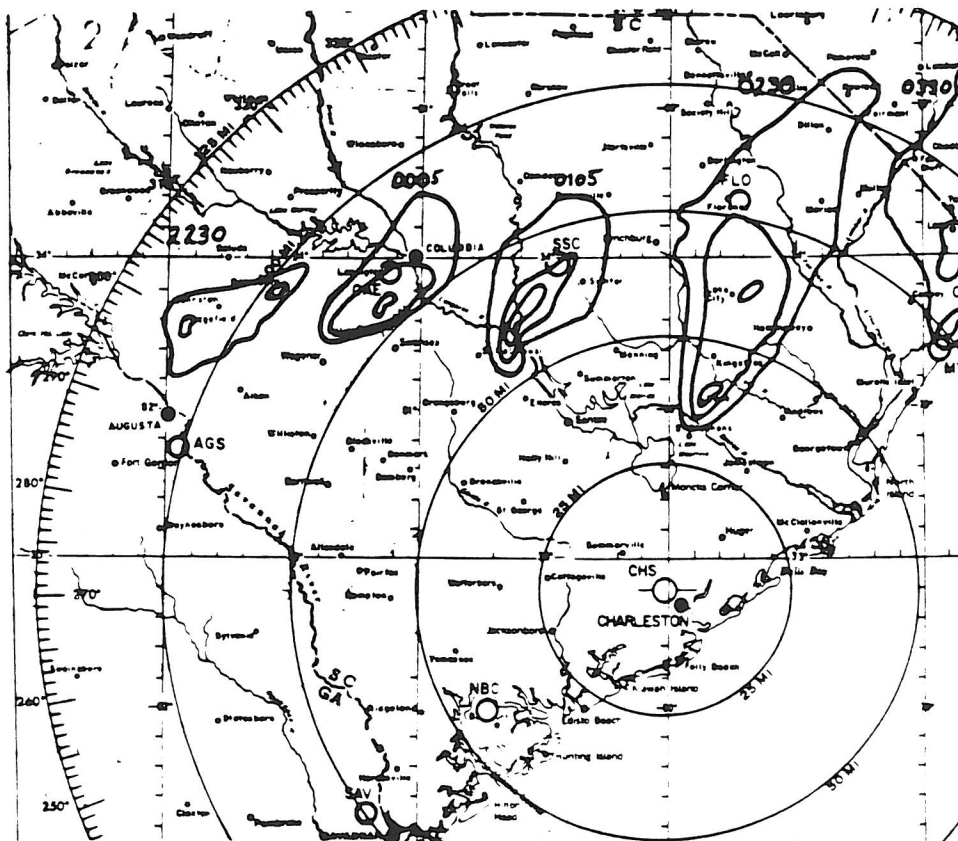
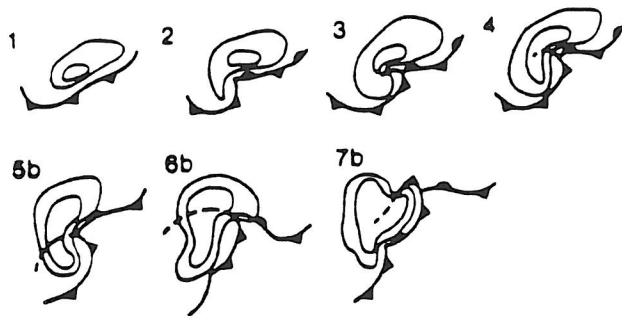
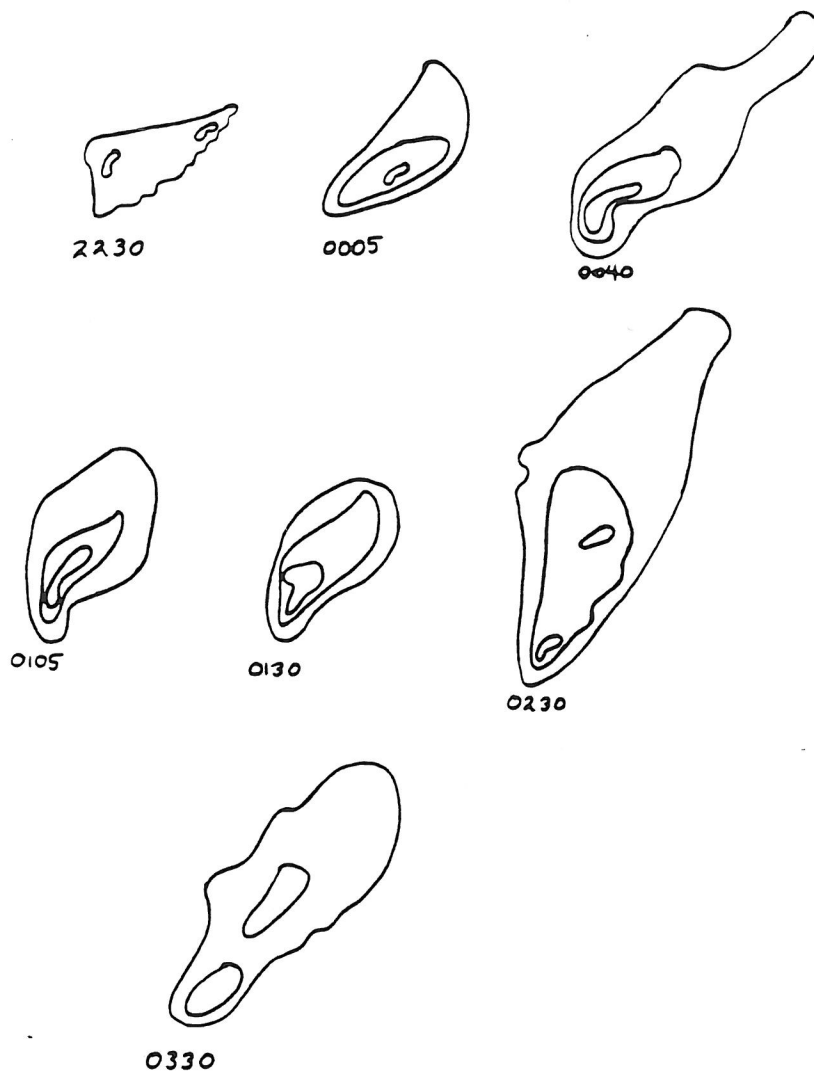


Figure 2. Radar reflectivity ( $0.5^\circ$  elevation) time series from the WSR-57 at CHS. VIP levels 1, 3, and 5 are contoured.



**Figure 3.** A composite life cycle (1-7b) identified with HP supercells (from Moller et al. 1990). VIP levels contoured as in Figure 2.



**Figure 4.** Life cycle of the March 13-14, 1991, South Carolina HP supercell as seen from the WSR-57 at CHS.

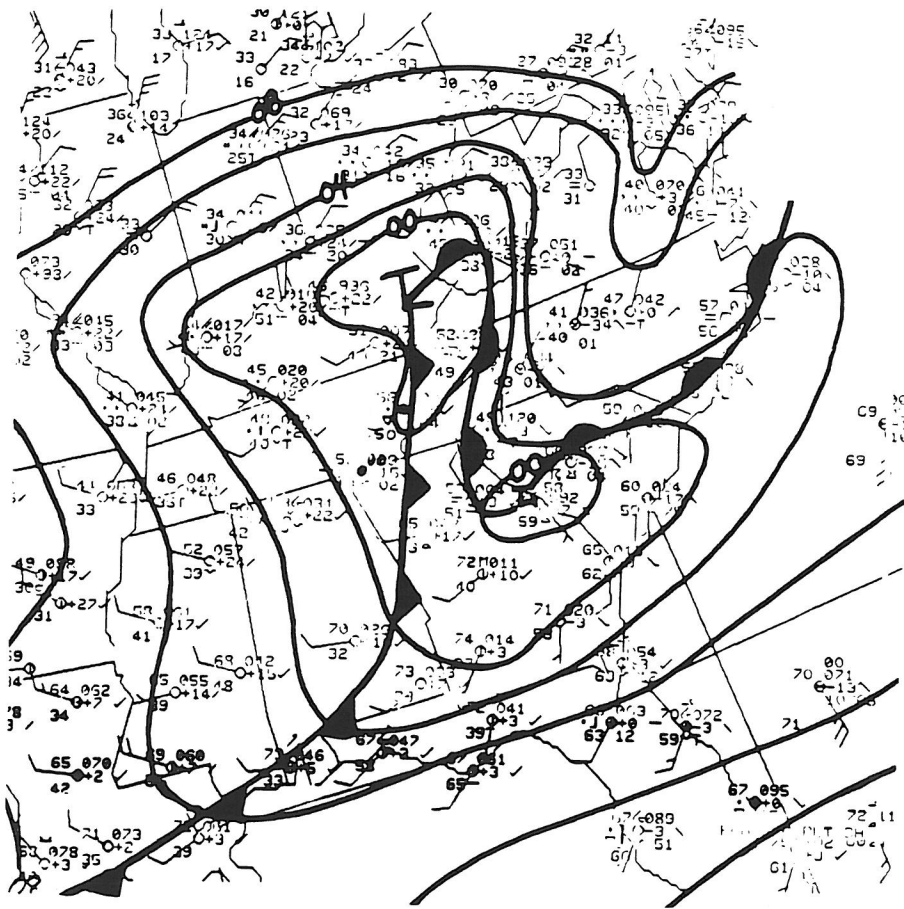


Figure 5. Surface analysis for 0000 UTC, March 14, 1991.

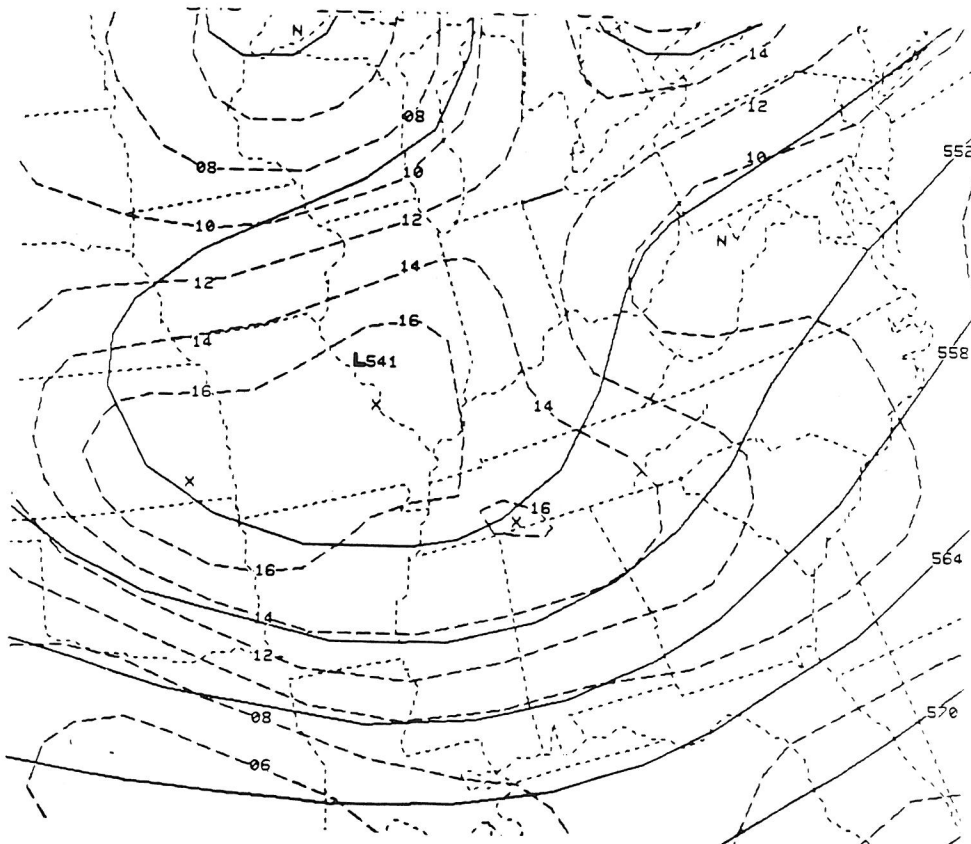


Figure 6. 500 mb heights and vorticity for 0000 UTC, March 14, 1991.

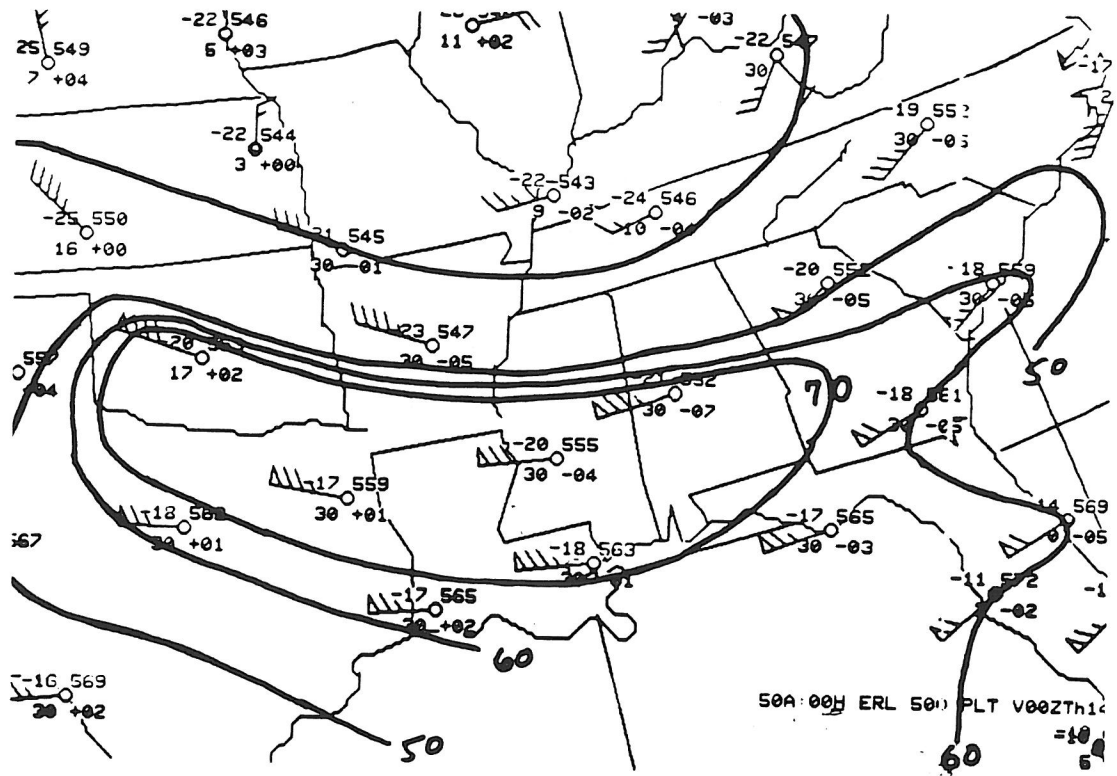


Figure 7. 500 mb plot and isotachs for 0000 UTC, March 14, 1991.

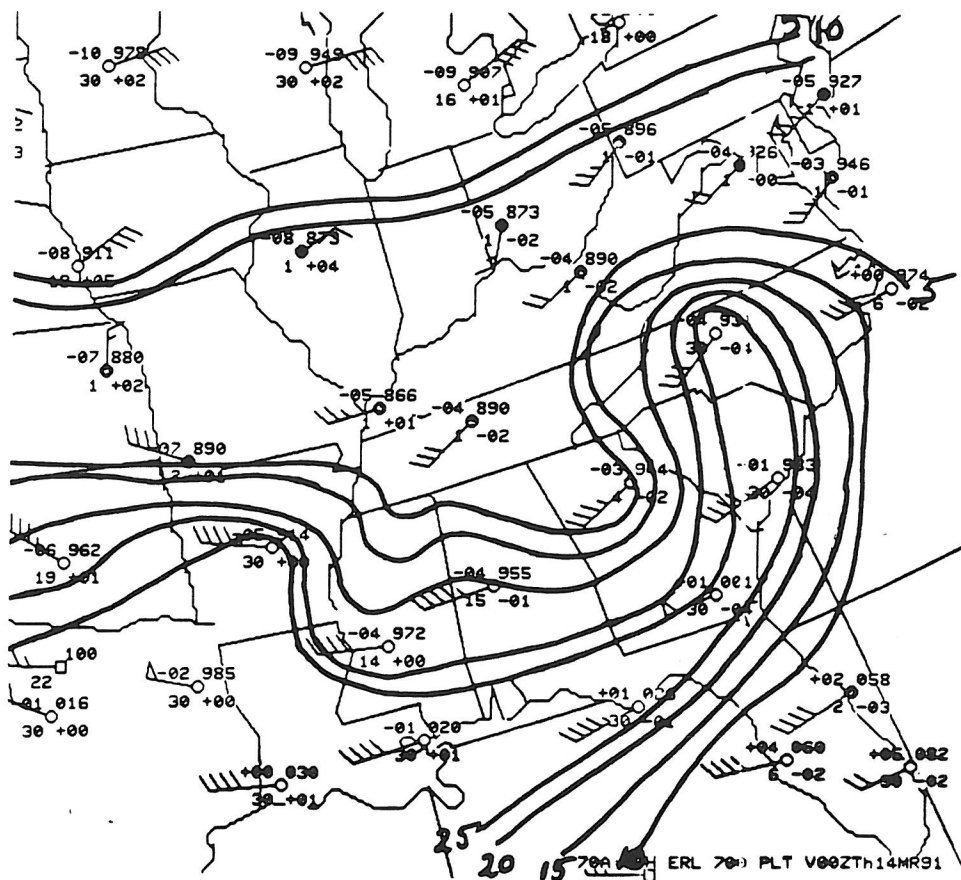


Figure 8. 700 mb plot and dew point depression analysis ( $^{\circ}\text{C}$ ) for 0000 UTC, March 14, 1991.

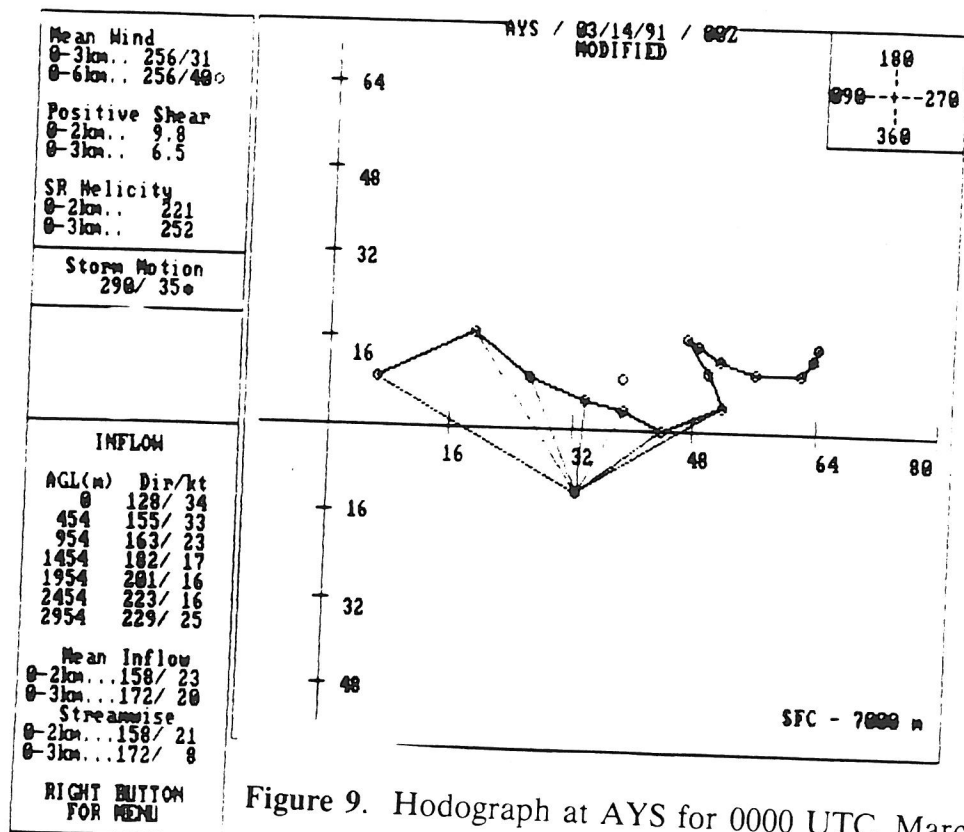


Figure 9. Hodograph at AYS for 0000 UTC, March 14, 1991.

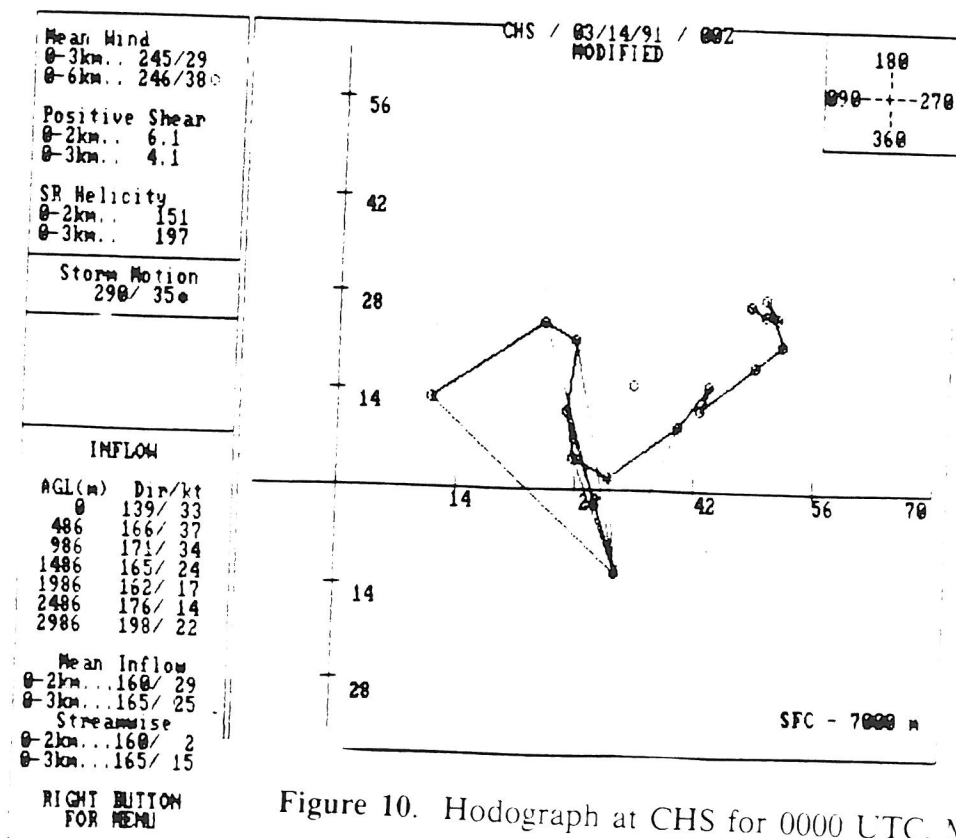


Figure 10. Hodograph at CHS for 0000 UTC, March 14, 1991.

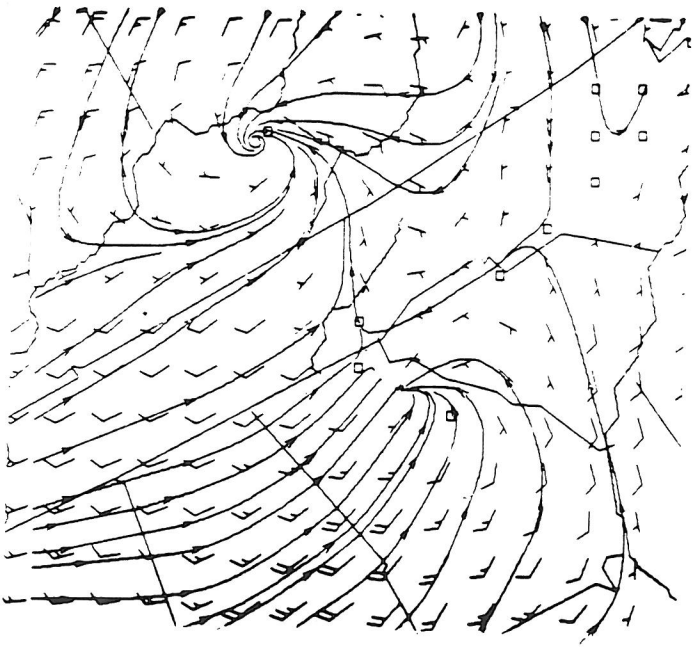


Figure 11a. Surface streamline and wind plot for 2200 UTC, March 13, 1991.

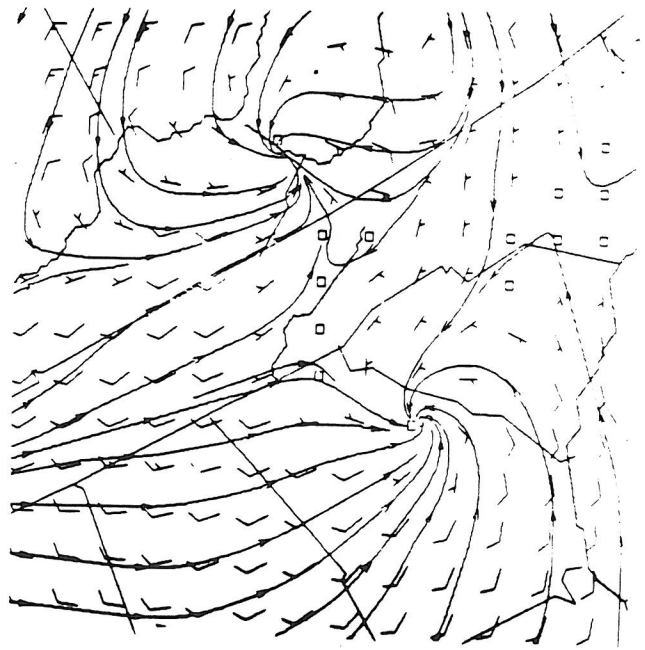


Figure 11b. Surface streamline and wind plot for 0000 UTC, March 14, 1991.

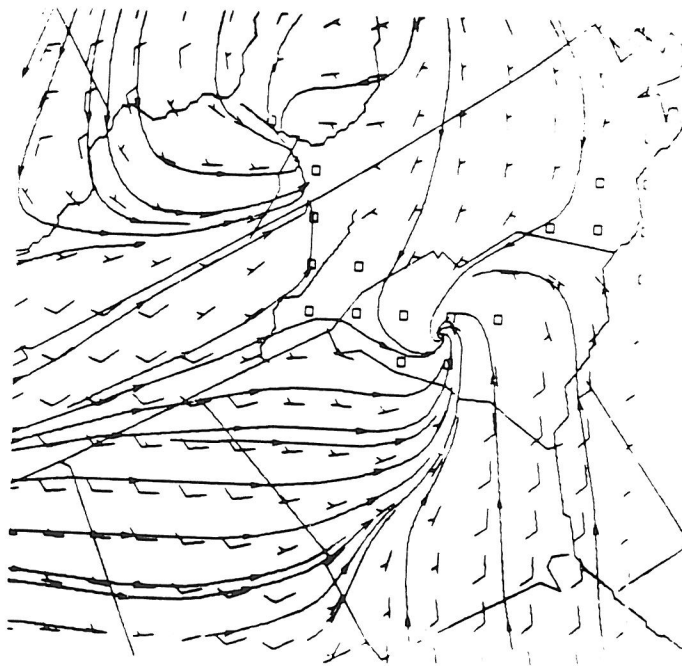


Figure 11c. Surface streamline and wind plot for 0200 UTC, March 14, 1991.

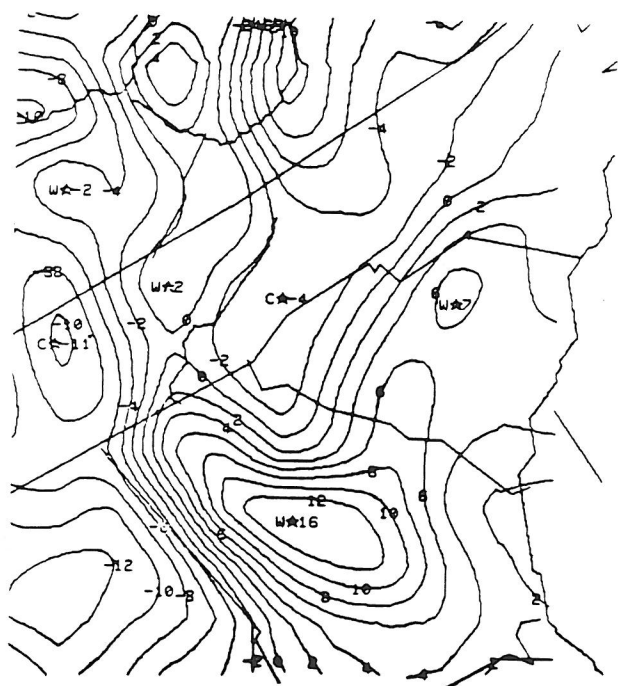


Figure 12. Surface potential temperature advection ( $^{\circ}\text{F hr}^{-1}$ ) for 2100 UTC, March 13, 1991.

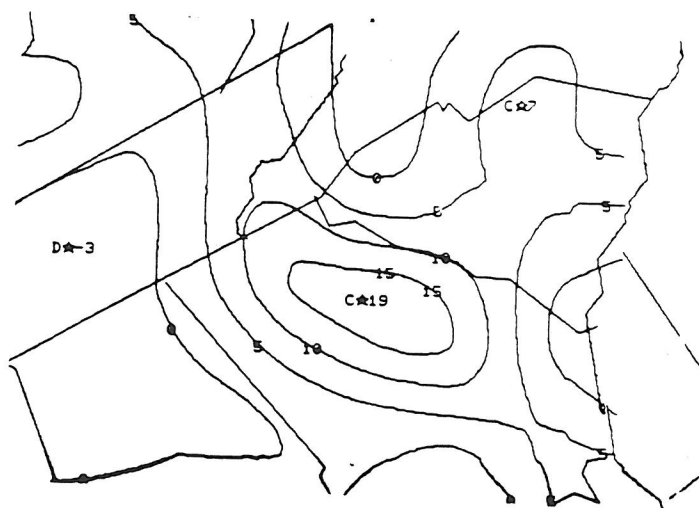


Figure 13. Surface moisture flux convergence ( $\text{g kg}^{-1} \text{hr}^{-1}$ ) for 2200 UTC, March 13, 1991.



Figure 14. Cap strength ( $^{\circ}\text{C}$ ) for 2200 UTC, March 13, 1991.

